Article

The Role of Vibrational Anharmonicity in the Computational Study of Thermal Spin Crossover

Jianfang Wu [1], Carmen Sousa [2,*] and Coen de Graaf [1,3]

[1] Departament de Química Física i Inorgànica, Universitat Rovira i Virgili, Marcel·lí Domingo 1,
    43007 Tarragona, Catalonia, Spain
[2] Departament de Ciència de Materials i Química Física, Institut de Química Teòrica i Computacional,
    Universitat de Barcelona, C/ Martí i Franquès 1, 08028 Barcelona, Catalonia, Spain
[3] ICREA, Passeig Lluís Companys 23, 08010 Barcelona, Catalonia, Spain
*   Correspondence: c.sousa@ub.edu

check for
updates

Abstract: Spin crossover in transition metal complexes can be studied in great detail with computational chemistry. Over the years, the understanding has grown that the relative stability of high-spin (HS) versus low-spin (LS) states is a subtle balance of many factors that all need to be taken into account for a reliable description. Among the different contributions, the zero-point energy (ZPE) and the entropy play key roles. These quantities are usually calculated assuming a harmonic oscillator model for the molecular vibrations. We investigated the impact of including anharmonic corrections on the ZPE and the entropy and indirectly on the critical temperature of spin crossover. As test systems, we used a set of ten Fe(II) complexes and one Fe(III) complex, covering different coordination modes (mono-, bi-, and tri-dentate ligands), decreasing coordination number upon spin crossover, coordination by second- and third-row atoms, and changes in the oxidation state. The results show that the anharmonicity has a measurable effect, but it is in general rather small, and tendencies are not easily recognized. As a conclusion, we put forward that for high precision results, one should be aware of the anharmonic effects, but as long as computational chemistry is still struggling with other larger factors like the influence of the environment and the accurate determination of the electronic energy difference between HS and LS, the anharmonicity of the vibrational modes is a minor concern.

Keywords: spin crossover; iron complexes; vibrational frequencies; transition temperature; DFT; anharmonicity

1. Introduction

Transition metal systems in which the metal atom can display various spin states are the prototypical examples of spin crossover (SCO) materials. These systems can undergo a transition from a low-spin (LS) to a high-spin (HS) state upon a variation of temperature or pressure, or by irradiation with light, or application of magnetic fields. The phenomenon of thermal spin crossover, that is the thermally-induced transition from an LS state predominating at low temperatures to an HS state at higher temperatures, was firstly reported by Cambi et al. [1,2] in the 1930s, and picked up again almost 40 years later. Ever since, the interest in SCO materials has continuously increased due to the potential applications as molecular switches in nanoscale devices. Later, the discovery of spin transition controlled by light irradiation opened the possibility of exploring the use of these systems as optically-switchable devices. Indeed, the so-called light-induced excited spin state trapping (LIESST) [3–6] effect allows the population at low temperatures of a metastable HS state by irradiating

into the absorption bands of the LS state. Moreover, in some systems, the process is reversible; therefore, irradiating the HS, the LS state is again populated.

Although SCO has been observed in transition metal complexes containing different metals and oxidation states, the Fe(II) containing complexes in an octahedral coordination are the most common systems and are considered to be the archetype of SCO complexes. For these systems, the LS is a singlet state, whereas the HS state of maximum spin multiplicity corresponds to a quintet state. Upon spin transition, the formal occupation of the anti-bonding orbitals increases by two electrons, from an LS (t_{2g}^6) configuration to an HS ($t_{2g}^4 e_g^2$), thus weakening the Fe(II)-ligand bonds. This effect causes important modifications in the coordination environment of the Fe(II) metal, mainly affecting the metal-ligand bond lengths and angles, and explains the changes observed in the crystal structure and crystal volume under SCO. For instance, in Fe(II) complexes including nitrogen ligands, the Fe(II)-N bond lengths increase on average by 0.2 Å, which implies around 10% of variation in the distance. The large structural changes accompanying the spin conversion have important effects on the vibrational spectra of the molecular complexes and on the lattice dynamics of the crystal. In fact, the vibrational frequencies related to the first coordination sphere of the metal decrease significantly on going from the LS to the HS state as a consequence of the weakening of the Fe-ligand bond.

Traditionally, the thermal spin crossover process has been schematically depicted as a one-dimensional potential energy diagram where the LS and HS states are represented within the harmonic approximation and the reaction coordinate corresponds to the totally symmetric normal mode. A key parameter for the characterization of SCO systems is the zero-point corrected energy difference between the HS and LS states, ΔH_{HL}^{ZPE}. In SCO materials, the LS-HS energy difference is small, typically below 2000 cm^{-1}. However, this property is in many cases difficult to access by experimental techniques. In turn, the transition temperature, $T_{1/2}$, defined as the temperature where LS and HS states are equally populated, can be determined experimentally by magnetic susceptibility measurements, Mössbauer spectroscopy, or calorimetric experiments [7–10]. For some systems, a hysteresis loop can be observed due to a difference in the transition temperature by heating from the LS to the HS and by the reverse cooling process. SCO materials showing transition temperatures in the room temperature range are the most suitable for real technological applications.

Under thermodynamic equilibrium conditions, where the variation of Gibbs energy equals zero, the transition temperature can be written as:

$$T_{1/2} = \frac{\Delta H_{HL}^{ZPE}}{\Delta S_{HL}(T_{1/2})} \tag{1}$$

where the enthalpy difference between the HS and LS states is assumed to be temperature independent and $\Delta S_{HL}(T_{1/2})$ is the variation of entropy between the HS and LS states at the corresponding transition temperature. The entropy increases on going from the LS to the HS state, and its value significantly changes with the temperature. Hence, the LS to HS conversion is considered an entropy-driven spin transition. For octahedral Fe(II) complexes with N-ligands, the ΔS_{HL} values normally range within 35–80 J K^{-1} mol^{-1}. By a great amount, the vibrational contribution is the largest portion of ΔS_{HL}; the electronic contribution arising from the change of spin multiplicity being a constant value of 13.38 J K^{-1} mol^{-1} and the rotational contribution notably minor. Moreover, previous studies based on Raman and IR spectroscopy [11] and by a combination of these techniques with density functional theory (DFT) calculations [12–14] demonstrated that the vibrational part of ΔS_{HL} is recovered by the low-energy vibrational modes, approximately 20% of the vibrations. Among these, the 15 modes involving the FeN$_6$ core account for about 75% of ΔS_{HL}.

The previous discussion stresses the importance of the vibrational contribution in both the value of the energy difference between the LS and HS states, ΔH_{HL}, through the vibrational zero point energy (ZPE) correction, and in the entropy change accompanying the spin transition, ΔS_{HL}. From the theoretical point of view, both properties, ΔH_{HL} and ΔS_{HL}, can be computed in a straightforward manner, and therefore, the transition temperature, $T_{1/2}$, can be estimated following Equation (1). In fact,

in the last few years, various theoretical studies aimed at determining the transition temperature have been published. Cirera and Paesani [15] computed the transition temperature in three octahedral Fe(II)-styrylpyridine complexes using several functionals within the DFT approach. The computed values of $T_{1/2}$ turned out to be around 50 K larger than the experiment. In these calculations, however, the ZPE correction in ΔH_{HL} was not included. Alternatively, Rudavskyi et al. [16] employed a mixed approach in which the ΔH_{HL} was computed by multiconfigurational wave function calculations, while the optimized geometries and harmonic vibrational frequencies were calculated within the DFT framework. In this work, it was shown that to get reliable values of ΔH_{HL}, inclusion of the ZPE correction, which stabilizes the HS state, is mandatory. Lately, a study of a set of twenty Cr, Mn, Fe, and Co complexes with several DFT functionals including dispersion, ZPE, and relativistic corrections showed only a qualitative estimation of the transition temperature [17].

A particular issue in the theoretical study of SCO materials is the precision in the calculation of the LS-HS energy difference. It is currently well-known that this quantity is highly dependent on the functional of choice, whereas in general, structural parameters and vibrational spectra do not significantly vary within the diverse DFT methods. Several studies have been performed in order to search the most suitable functional and/or establish the optimal amount of exact exchange in hybrid functionals to describe SCO complexes accurately [18–22]. Recently, some studies in various Fe(II) compounds [17,23,24] have shown that the hybrid meta-GGATPSSh functional [25], containing 10% exact Hartree–Fock exchange, yield accurate energies between different spin states. On the other hand, ab initio multireference wave function calculations based on the CASSCF/complete active space second-order perturbation theory (CASPT2) methodology [26–29] or coupled cluster (CC) calculations [30] have been proven to describe different spin states and their relative energy difference successfully in several transition metal complexes, irrespective of the metal involved and the oxidation state considered. Although these calculations are computationally more expensive than those based on DFT, and thus often restricted to relatively small systems, they avoid the cumbersome question of searching for the appropriate functional.

All the computational studies performed to estimate the entropy variation, ΔS_{HL}, and the transition temperature, $T_{1/2}$, were based on the harmonic model to describe the molecular vibrations. Here, we aim to explore the effect of the anharmonic terms on the SCO process and, in particular, the effect on the energy difference between the LS and HS states, the change of entropy accompanying the spin transition, and on the final transition temperature.

As has become apparent from the above discussion, molecular vibrations are essential to the understanding of SCO, but there are more research areas where molecular vibrations and the degree of anharmonicity are at the center of interest. IR, Raman [31], and even UV-Vis [32] spectra cannot always be fully explained without the inclusion of anharmonic corrections. Second-order vibrational perturbation theory [33] provides researchers with an efficient tool to study in great detail the underlying mechanisms that give rise to the richness of features in the experimental spectra. Recently, molecular vibrations have become also extremely important in the field of single molecule magnets (SMM). Many studies have established that the energy barrier along the path from M_S^{max} to $-M_S^{max}$ does not (directly) relate to the blocking temperature, and other relaxation mechanisms are to be investigated [34]. One of them is based on spin-vibration (either phonons or molecular vibrations) coupling [35,36], which appears to be the dominant mechanism in the record SMMs based on dysprosium [37,38]. The description of the spin-vibration coupling has recently been extended with the inclusion of anharmonic terms, which turn out to be essential to explain the relaxation mechanism at higher temperatures [39].

To quantify the importance of anharmonicity in the context of SCO, several iron compounds have been considered, and for all of them, displacements along all the normal vibrational modes of

the complex have been explored. By fitting the energy variation of the system along the vibrational coordinate of each normal mode to the fourth-order polynomial:

$$E(Q_i) = a\,Q_i^2 + bQ_i^3 + cQ_i^4, \tag{2}$$

anharmonic corrections can be extracted, and as a result, the influence on the ZPE, ΔS_{HL} and $T_{1/2}$ can be estimated.

Figure 1 illustrates the effect of the cubic (b) and quartic (c) corrections on the harmonic curve $E(Q) = a\,Q^2$ with $a = 1$, displayed in red. The first two panels of the upper row show that the cubic correction introduces asymmetry in the potential energy curve, tightening the curve on the right (left) and widening it on the left (right) for b larger (smaller) than zero. The next two panels show how the introduction of a quartic correction maintains the symmetry, but narrows (loosens) the curve for c larger (smaller) than zero. In the lower row, the combined effect of the two corrections is shown. We have taken the limiting case where the two corrections are similar in magnitude; in other cases, the upper row applies. When b and c have the same sign, their effect is largely canceled on one side of the curve, while it rises more steeply on the other side. For opposite signs, the effect is again canceled on one side, but the curve is now opened on the other side, resulting in a potential energy curve that resembles to some extent a Morse potential.
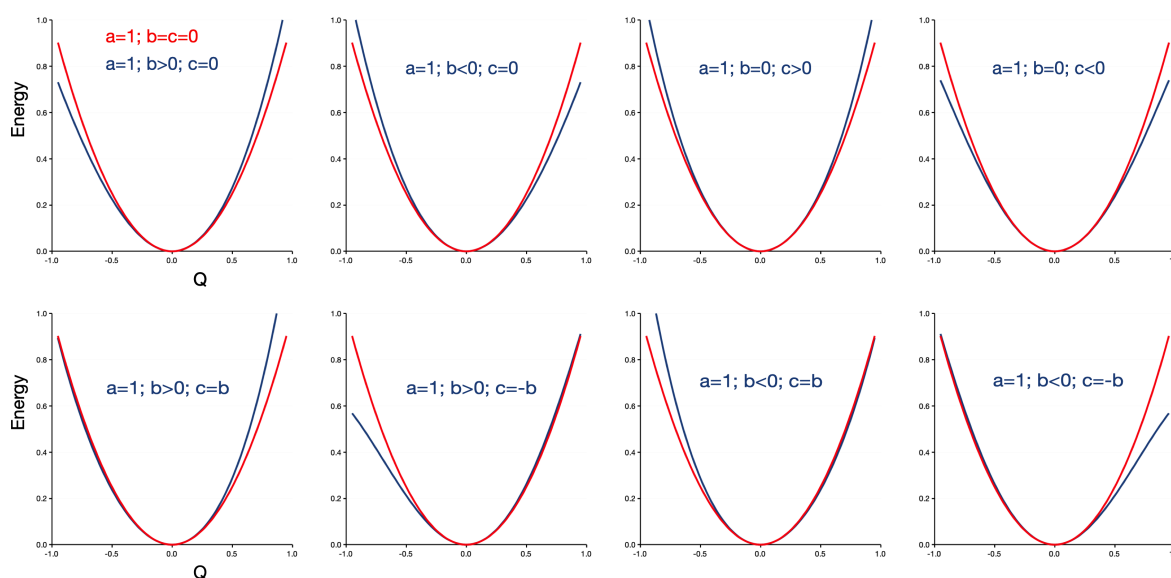

Figure 1. Influence of the cubic (b) and quartic (c) corrections (in blue) on the harmonic potential energy curve (in red). $|b|$ and $|c|$ are 0.2 when non-zero.

Alternative methods to estimate anharmonic effects are mostly based on (numerical) third- and fourth-order derivatives [40–43]. However, the ab initio variant of these methods is computationally prohibitive for typical SCO complexes, much larger than the benchmark system presented in [43], the protonated dipeptide GlyGlyH$^+$, for which the calculation took 56 wall-clock hours on 2000 cores. The much faster hybrid variants are also not straightforwardly applicable due to the lack of general and accurate force fields for transition metal complexes.

Eleven different iron complexes have been studied, which are shown in Figure 2. These encompass the two oxidation states of iron, Fe(II) and Fe(III), and various arrangements of the Fe first-neighbor coordination. First, the model system [Fe(NCS)$_2$(NCH)$_4$] was studied as a test case [44]. Thereafter, we considered a set of six Fe(II) complexes with an octahedral FeN$_6$ coordination, which was studied in a previous work [16]. These include two complexes with monodentate ligands, [Fe(mtz)$_6$]$^{2+}$ and [Fe(iso)$_6$]$^{2+}$ (with mtz = 1-methyltetrazole and iso = isoxazole), three bidentate ligand complexes, [Fe(phen)$_2$(NCS)$_2$], [Fe(pic)$_3$]$^{2+}$, and [Fe(bpy)$_3$]$^{2+}$ (where phen = 1,10-phenanthroline,

pic = 2-picolylamine, and bpy = 2,2′-bipyridine), and a tridentate ligand Fe(II) complex, $[Fe(terpy)_2]^{2+}$, with terpy = 2,2′:6′,2″-terpyridine. The first four complexes of this set are susceptible to undergoing SCO, whereas the $[Fe(bpy)_3]^{2+}$ and $[Fe(terpy)_2]^{2+}$ systems are LS compounds where SCO is only possible by irradiation of light. In particular, the $[Fe(phen)_2(NCS)_2]$ system has been extensively studied both experimentally [11,45,46] and by theoretical calculations [13,47,48] as a representative example of a Fe(II) SCO complex with an octahedral FeN_6 coordination. For this system, thermal spin conversion occurs at 176 K, and the SCO enthalpy is estimated to be 8.60 ± 0.14 kJ mol^{-1}. Next, two six-coordinated Fe(II) complexes where the central iron is bonded to sulfur-contained ligands were considered. In such a way, the effect in the anharmonic vibrations of third-row atoms as first-nearest neighbors can be explored and compared to the usual second-row C, N, or O atoms. Specifically, the $[Fe(CO)(N_HS_4)]$ and $[Fe(NH_3)(N_HS_4)]$ complexes, with $N_HS_4{}^{2-}$ = 2,2′-bis(2-mercaptophenylthiol)diethylamine dianion, have been studied [20,49,50]. Subsequently, a Fe(II) heptacoordinated complex has been considered, the dicyano[2,13-dimethyl-6,9- dioxa-3,12,18-triazabicyclo[12.3.1]octadeca-1(18),2,12,14,16-pentaene]iron(II) monohydrate compound, $[FeL(CN)_2] \cdot H_2O$ [51]. In this system, SCO is concomitant with a structural change from a hepta-coordination for the HS to a hexa-coordination in the LS. Thermal spin crossover by cooling is observed at 155 K. Finally, a compound containing Fe(III) in a six-coordinated surrounding was included in this study, the $[Fe(acac)_2trien]^+$ complex with acac = acetylacetonate-triethylenetetramine [18,52]. This complex has a sextet HS and a doublet LS, and the HS-LS enthalpy was determined for various solvents, with values in the range 700–1172 cm^{-1} [52].
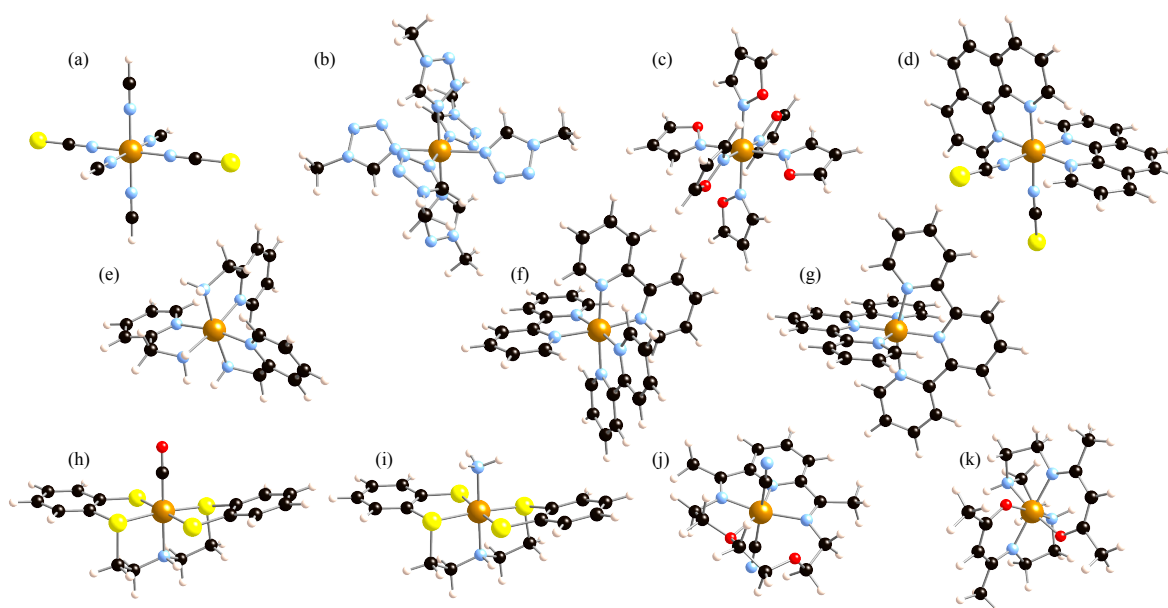

Figure 2. Molecular complexes investigated in this study: $[Fe(NCS)_2(NCH)_4]$ (**a**), $[Fe(mtz)_6]^{2+}$ (**b**), $[Fe(iso)_6]^{2+}$ (**c**), $[Fe(phen)_2(NCS)_2]$ (**d**), $[Fe(pic)_3]^{2+}$ (**e**), $[Fe(bpy)_3]^{2+}$ (**f**), $[Fe(terpy)_2]^{2+}$ (**g**), $[Fe(CO)(N_HS_4)]$ (**h**), $[Fe(NH_3)(N_HS_4)]$ (**i**), $[FeL(CN)_2] \cdot H_2O$ (**j**), and $[Fe(acac)_2trien]^+$ (**k**). Fe is in the center of the complexes, represented by a light brown sphere. Black spheres represent C; blue is N; red is O; yellow is S; and pink is H.

2. Results and Discussion

To start the discussion of the results, we first focus on the model complex $[Fe(NCS)_2(NCH)_4]$ to illustrate the differences between harmonic potential energy curves (given by Equation (2) with $b = c = 0$ and $a = 0.5\omega_i$, the harmonic vibrational frequency of mode i) and those that are obtained by fitting the calculated data to the quartic expression of Equation (2). The normal mode of the LS state corresponding to the in-plane movement of the NCH ligands has a harmonic frequency of

147.3 cm^{-1}. Close to the equilibrium geometry, the NCH groups have very little interaction, but when they approach each other, the repulsion increases and the energy rises faster than predicted by the harmonic approximation, as can be seen on the right part of Figure 3. Due to the symmetry in the plane, this faster rising is equal for positive and negative displacements defined by the coordinate Q. Hence, a sizeable quartic contribution ($c = 2.13$) arises when the computed energies are fitted, while the cubic contribution stays very close to zero. The quadratic term (the anharmonic frequency) becomes 148.6 cm^{-1}, slightly larger than the harmonic frequency. Therefore, the ZPE is increased, and the shape of the fitted curve also makes the strict regular spacing between the vibrational levels be lost, although the effect is not dramatic. The energy difference between ν_0 and ν_1 is 148.7 cm^{-1}, and $\Delta E_{\nu_{14}-\nu_{15}}$ equals 150.4 cm^{-1}.
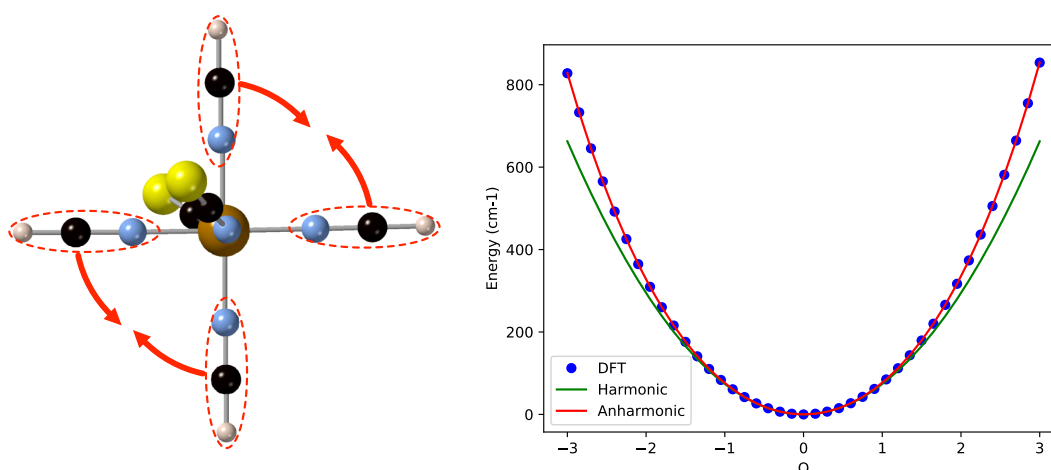

Figure 3. **Left**: In-plane NCH bending mode of the low-spin (LS) state of [Fe(NCS)$_2$(NCH)$_4$]. **Right**: Comparison of the harmonic potential energy curve (in green) and the calculated energies (blue dots) fitted with a quartic expression (red line).

As an example of cubic corrections to the harmonic approximation, we mention the vibrational mode mainly characterized by the off-center movement of Fe as shown on the left of Figure 4. When the iron moves away from the NCS groups (in the direction of the red arrow), the energy rises less rapidly than when it moves towards these groups. The harmonic frequency of this mode is 343.7 cm^{-1}, and the fitting of the DFT energies introduces a cubic term of -13.6 and an anharmonic frequency of 347.8 cm^{-1}. The quartic term is small in this case. The ZPE is again larger, but now, the spacing between the vibrational levels of the anharmonic curve remains constant within 0.1 cm^{-1}.

The anharmonic correction to the ZPE is small in all 56 normal modes of the LS state of the model complex, but positive in almost all cases and finally adds up to a significant contribution of 159.7 cm^{-1}. The vibrational entropy term $T\Delta S$ at T = 298 K within the harmonic approximation is 85.5 kJ mol^{-1}, decreasing to 79.0 kJ mol^{-1} when the anharmonic terms are taken into account, which is in line with the general tendency of larger ZPE for the anharmonic curves.

Table 1 summarizes how the ZPE is affected by the anharmonicity of the potential energy curves for the ten other complexes. Positive values indicate an increased ZPE (overall hardening of the vibrational modes), while negative numbers indicate that the ZPE has been lowered by the introduction of the anharmonic terms, that is a net softening of the modes. The third column shows the effect on the HS-LS ZPE difference to be added to the electronic energy difference between the two states. Except for [FeL(CN)$_2$]·H$_2$O, the effect on the HS-LS energy difference is limited to a correction smaller than 200 cm^{-1}. Ordering the complexes with a Fe(II)N$_6$ core by increasing contribution of the anharmonicity to the ZPE difference between HS and LS, it becomes apparent that the coordination mode of the ligand is likely to play a role in the importance of the anharmonicity. [Fe(terpy)$_2$]$^{2+}$, with two tridentate ligands, has the largest negative contribution, followed by [Fe(bpy)$_3$]$^{2+}$, three bidentate

ligands, and [Fe(phen)$_2$(NCS)$_2$] with two bidentate ligands. [Fe(pic)$_3$]$^{2+}$ has also bidentate ligands, but these are much less rigid than the phenanthroline or bipyridine ligands of the other two complexes. The two monodentate complexes, [Fe(mtz)$_6$]$^{2+}$ and [Fe(iso)$_6$]$^{2+}$, have a small negative contribution and a moderate positive one, respectively. This difference may be related to the size of the ligands; 1-methyl-tetrazole has significantly more atoms than isoxazole. Inserting the other complexes in trend is more difficult. [FeL(CN)$_2$]·H$_2$O increases the coordination of Fe from six to seven upon the LS to HS transition, which induces large changes in the vibrational modes. [Fe(acac)$_2$trien]$^+$ contains a Fe(III) ion, and the two complexes with the N$_H$S$_4$ ligand have four sulfur atoms in the first coordination sphere of Fe. These two compounds differ by the axial ligand. With CO (a π acceptor ligand), the system is LS, and with NH$_3$, a σ-donor, the ground state of the complex is an HS state. These substantial differences make the comparison with the other complexes more intricate.
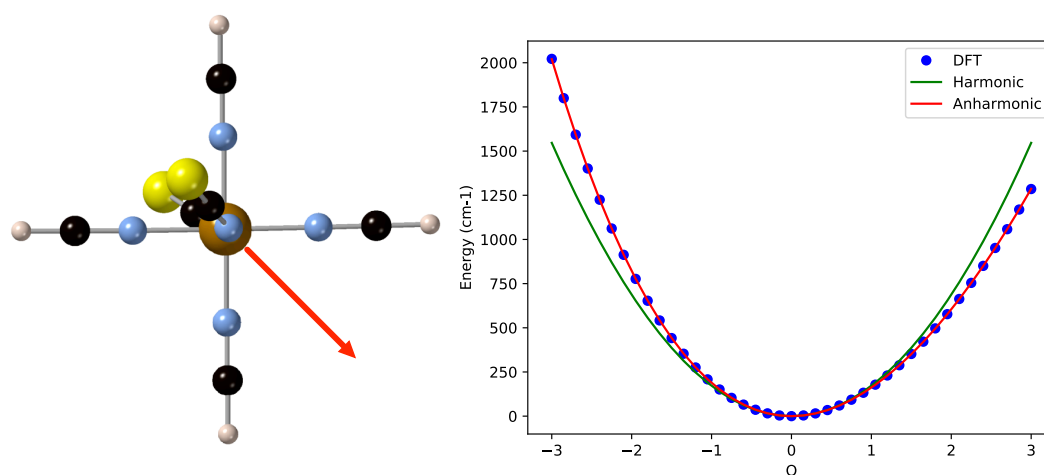

Figure 4. (**Left**) Off-center Fe displacement vibrational mode of the LS state of [Fe(NCS)$_2$(NCH)$_4$]. (**Right**) Comparison of the harmonic potential energy curve (in green) and the calculated energies (blue dots) fitted with a quartic expression (red line).

Table 1. Contribution of the anharmonicity to the zero point energy with respect to the harmonic value (in cm^{-1}). HS, high-spin.

System	LS	HS	HS-LS
[Fe(mtz)$_6$]$^{2+}$	690	645	−46
[Fe(iso)$_6$]$^{2+}$	−312	−160	152
[Fe(phen)$_2$(NCS)$_2$]	298	177	−122
[Fe(pic)$_3$]$^{2+}$	97	142	45
[Fe(bpy)$_3$]$^{2+}$	31	−143	−174
[Fe(terpy)$_2$]$^{2+}$	123	−69	−192
[Fe(CO)(N$_H$S$_4$)]	1014	1166	153
[Fe(NH$_3$)(N$_H$S$_4$)]	213	247	35
[FeL(CN)$_2$]·H$_2$O	667	−191	−857
[Fe(acac)$_2$trien]$^+$	511	446	−65

The second property that is affected by the anharmonic contributions to the potential energy curves is the vibrational entropy. Table 2 lists the most important results to illustrate the effect of anharmonicity on the energetics of the complexes studied here. In addition to the ZPE and the entropy, we also list the electronic energy difference between HS and LS (ΔH_{HL}) and the ZPE corrected energy ($\Delta H_{\text{HL}}^{\text{ZPE}}$). As mentioned in the Introduction, precise estimates of the latter quantity

are difficult to calculate. CASPT2 has been shown in several studies to provide reasonable estimates, but this comes at the cost of having to reoptimize the first coordination sphere of the metal ion. Optimal CASPT2 Fe-Ligand distances are systematically shorter than those obtained with DFT, the difference being typically between 0.05 Å and 0.08 Å. This geometrical reorganization has a marked effect on ΔH_{HL}, and if one wants to stick to the standard definition of the zeroth-order CASPT2 Hamiltonian, the optimization of the first coordination sphere is mandatory; ΔH_{HL} calculated on the DFT geometries does not in general give the best estimates. Alternatively, one could increase the so-called IPEA parameter in $\hat{H}^{(0)}$, but this introduces a certain arbitrariness into the calculation that should ideally be avoided. For the compounds that were studied previously in [16], all with a Fe-N$_6$ coordination, we list the CASPT2 values for ΔH_{HL}. For the new complexes, we limited ourselves to the TPSSh estimates, because the optimization of the first coordination sphere becomes very laborious for these complexes since the scan along the symmetric stretching frequency (as done in the previously studied complexes) is not adequate for determining the optimal Fe-ligand distances. The coordination sphere is too asymmetric for this, and one would have to perform a two- or even three-dimensional exploration of the potential energy surface, which goes well beyond the scope of this study; the electronic energy difference ΔH_{HL} is not directly influenced by the anharmonicity. TPSSh gives the correct spin multiplicity for all complexes but one. [Fe(NH$_3$)(N$_H$S$_4$)] is reported to be a high-spin molecule, but the TPSSh energies indicate an LS ground state. A series of single point CASPT2 calculations along the one-dimensional interpolation path between HS and LS optimized geometries resulted in an HS ground state ($\Delta H_{HL} = -1165$ cm^{-1}). However, note that this is only a starting point and that a definite CASPT2 estimate requires the independent optimization of the Fe-S, Fe-NH$_3$, and the Fe-NR$_2$ distances in this particular case.

Table 2. TPSSh values of the HS-LS energy difference, ΔH_{HL}, zero point energy (ZPE) contribution, ΔZPE_{HL}, zero point corrected HS-LS energy difference, ΔH_{HL}^{ZPE}, and entropy variation at 298 K, ΔS_{HL}, computed using the harmonic and anharmonic approximations. Energies in cm^{-1} and entropy variation in J K^{-1} mol^{-1}.

	ΔH_{HL}	ΔZPE_{HL}		ΔH_{HL}^{ZPE}		ΔS_{HL} (298 K)	
		Harm	**Anharm**	**Harm**	**Anharm**	**Harm**	**Anharm**
[Fe(mtz)$_6$]$^{2+}$	1051 [a]	−966	−1012	85	39	88.5	83.8
[Fe(iso)$_6$]$^{2+}$	1062 [a]	−920	−68	142	294	87.9	147.1
[Fe(phen)$_2$(NCS)$_2$]	1362 [a]	−754	−875	608	487	60.8	23.1
[Fe(pic)$_3$]$^{2+}$	1320 [a]	−981	−937	339	383	68.4	66.8
[Fe(bpy)$_3$]$^{2+}$	5807 [a]	−515	−689	5292	5118	54.6	88.2
[Fe(terpy)$_2$]$^{2+}$	7919 [a]	−501	−692	7418	7227	59.5	84.2
[Fe(CO)(N$_H$S$_4$)]	9154	−867	−714	8287	8440	63.3	38.9
[Fe(NH$_3$)(N$_H$S$_4$)]	2595	−818	−783	1776	1811	78.0	65.0
[FeL(CN)$_2$]·H$_2$O	3998	−847	−1704	3151	2293	41.4	42.2
[Fe(acac)$_2$trien]$^+$	3642	−11	−877	2831	2766	38.8	36.8

[a]: complete active space second-order perturbation theory (CASPT2) values taken from [16].

Moving to the next column of Table 2, we see that the ZPE in the harmonic approximation adds another 500–1000 cm^{-1} to the HS-LS energy difference in favor of the HS state. The larger Fe-ligand distance leads to wider potential energy curves in the HS and hence to smaller ZPEs, reducing the HS-LS gap for LS molecules. The anharmonic effects introduce changes to the ΔZPE_{HL} on the order of 50–200 cm^{-1}, except for the much larger variation in [FeL(CN)$_2$]·H$_2$O caused by the change in coordination number, as discussed before. Adding the ZPE correction to the HS-LS energy difference greatly reduces the gap and results in small ΔH_{HL}^{ZPE} values for those complexes that are susceptible to SCO. The only missing aspect to complete the picture is the entropy contribution. To give an impression of how anharmonicity affects the entropy, the last two columns of Table 2 list the calculated variation

of entropy at T = 298 K for the series of complexes in the HS and LS states. Apart from the vibrational term, ΔS_{HL} also includes the electronic contribution to the entropy, a temperature independent term that only depends on the spin multiplicity of the HS and LS states. This term is equal to 13.38 J K^{-1} mol^{-1} for the Fe(II) complexes and 9.13 J K^{-1} mol^{-1} for the Fe(III) complex. For the first four molecules, the effect of anharmonicity on the ZPE is also reflected in the entropy at 298 K. When anharmonicity reduces ΔH_{HL}^{ZPE}, that is when the anharmonicity raises more (or lowers less) the ZPE in the HS than in the LS state, the entropy at 298 K increases more (or decreases less) in the HS state with respect to the LS state. This may at first sight lead to the conclusion that the entropy changes are fully governed by the ZPE, but the results for the other complexes show that the picture is more complicated and that the non-uniform level spacing also plays a role in the way in which anharmonicity affects the entropy. This effect is more complicated to analyze since it changes from vibration to vibration. As the entropy has contributions from all vibrational modes, we have not been able to find a simple reasoning to explain the tendency in the changes of the entropy upon the inclusion of anharmonic effects.

With the entropy and ZPE corrected for anharmonic effects, we are now ready to study its influence on the critical temperature for spin transition, $T_{1/2}$, for those complexes that show SCO behavior. Before discussing the results listed in Table 3, it is important to note that we do not pretend to give a precise number for the transition temperature. Although we account reasonably well for most of the factors related to the electronic structure of the complexes (ZPE, entropy, relativistic effects, etc.), the gas phase material model applied here is not sufficient to obtain a realistic estimate of $T_{1/2}$. However, this is not the aim of the study. Instead, the numbers listed in Table 3 do give some hints on how the anharmonicity affects the transition temperature. Following Equation (1), we have determined the critical temperature for SCO with and without anharmonic corrections by looking for the temperature at which $T\Delta S(T)$ is equal to ΔH_{HL}^{ZPE}. Table 3 lists the resulting $T_{1/2}$ and the variation in the entropy at that temperature.

Table 3. Computed values of the zero point corrected HS-LS energy difference, ΔH_{HL}^{ZPE}, entropy variation at $T_{1/2}$, $\Delta S_{HL}(T_{1/2})$, and transition temperature, $T_{1/2}$. Energies in cm^{-1}, temperature in K, and entropy variation in J K^{-1} mol^{-1}.

| | ΔH_{HL}^{ZPE} | | $\Delta S_{HL}(T_{1/2})$ | | $T_{1/2}$ | | Experiment | |
	Harm	Anharm	Harm	Anharm	Harm	Anharm	ΔH_{HL}^{ZPE}	$T_{1/2}$
$[Fe(mtz)_6]^{2+}$	85	39	34.8	26.5	30	19	120 [53]	78 [54]
$[Fe(iso)_6]^{2+}$	142	294	38.2	70.7	44	49	-	91 [55]
$[Fe(phen)_2(NCS)_2]$	608	487	54.4	22.0	134	264	719 [45]	176 [46]
$[Fe(pic)_3]^{2+}$	339	383	49.6	46.8	82	98	744 [56]	114–121 [57]
$[Fe(acac)_2trien]^+$	827	761	37.8	35.6	262	256	700–1200 [52]	-

The temperatures within the harmonic approximation are practically the same as in the previous study [16] despite the different functional (B3LYP versus TPSSh) and the larger basis for Fe (TZVP versus QZVPP). The inclusion of the anharmonicity introduces small changes in the critical temperature in four cases and affects quite significantly the transition temperature of the $[Fe(phen)_2(NCS)_2]$ complex. However, the presence of very low frequency vibrational modes in the latter molecule makes the comparison between harmonic and anharmonic somewhat delicate, since small changes in the interval used for fitting the DFT energies lead to substantial changes in the anharmonic parameters. The fitting procedure is much more robust for vibrations with higher frequencies, and the size of the interval does not have great influence on the other complexes.

3. Methods

All DFT calculations were performed with the Orca 4.1.1 code [58]. Geometry optimizations and frequency calculations were done with the TPSSh density functional and the Gaussian type basis sets of Weigend and Ahlrichs of the triple-ζ + polarization (def2-TZVP) quality for all atoms, but iron,

for which we applied a basis set of quadruple-ζ + double polarization quality (def2-QZVPP) [59]. The calculation of the exact Fock contribution was accelerated by applying the RIJCOSXapproximation developed by Neese and co-workers [60,61]. Tight convergence criteria and a fine grid for the numerical integration (grid5) were chosen to avoid numerical noise in the calculation of the vibrational frequencies, which has to be done by numerical differentiation. In a study of the anharmonic effects in a series of metallocenes by Latouche et al., it was shown that the choice of basis set and density functional is not of critical importance; all the different combinations studied gave basically the same anharmonic corrections [62].

The complete active space second-order perturbation theory (CASPT2) calculations of the adiabatic high-spin/low-spin energy difference were performed with Molcas 8.2 [63]. Following the conclusions of earlier studies [16,29], we applied ANO-RCCbasis sets with a (7s,6p,5d,4f,3g,2h) contraction for Fe, triple-ζ + polarization for the atoms in first coordination sphere, and double-ζ for the other atoms. The active space contained 12 orbitals (5 Fe-3d, a second d-shell, and the two ligand-σ orbitals) and 10 or 9 electrons for Fe(II) and Fe(III), respectively. This is the standard active space for (quasi-)octahedral third-row transition metal complexes with 5 or more electrons in the *d*-shell [26,27]. The standard zeroth-order Hamiltonian (IPEA = 0.25) was used and an imaginary level shift of 0.15 E_h added to the denominators to avoid the appearance of intruder states. All electrons were included in the treatment of the dynamic correlation except the deep-core electrons ($1s^2,2s^2,2p^6$ for Fe and S and $1s^2$ for C, N, and O). Since a full CASPT2 geometry optimization is out of reach for these molecules, we optimized the Fe-L distances by single-point calculations on a series of structures that interpolate between the DFT HS and LS state minima. Each point in this series was generated by a DFT geometry optimization in which only the Fe-L distances were fixed.

The effect of anharmonicity on the vibrational entropy and the zero point vibrational energy was estimated by the following procedure. After the calculation of the (harmonic) vibrational frequencies ω_i and the corresponding normal modes Q_i (the eigenvectors of the Hessian), we generated 40 geometries along all normal modes (%mtrkeyword of Orca) for the LS and HS states with a step size δQ_i that depended on ω_i. For the normal modes with ω smaller than 200 cm^{-1}, we applied a step size of $0.06 \cdot Q_i$, for $\omega > 2500$ cm^{-1} (C-H and N-H stretching vibrations), $\delta Q_i = 0.1 Q_i$, and for all the intermediate vibrations, we used a step size of 0.25 Q_i. The changes in the step size were applied to ensure a realistic interval of atom displacements in all vibrational modes avoiding too large energy increases at the largest Q_i. Next, DFT calculations were performed on these geometries, and the results were fitted with the polynomial of Equation (2) using the least squares fitting procedure of the SciPy library of Python. This analytical function defines $\hat{V}$ in the Hamiltonian $\hat{H} = \hat{T} + \hat{V}$, with $\hat{T}$ the kinetic energy operator. The Schrödinger equation was solved for the lowest 15 eigenvalues for each vibrational mode using the eigenvalue solver linalg.eigsh from SciPy. Even at the highest temperature considered, the population of the 15th level was low enough to have a negligible effect on the thermodynamic properties. The 15 eigenvalues were used to calculate the partition function Z_i and, subsequently, the total vibrational partition function Z as $\prod_i Z_i$, from which the entropy followed as $\Delta S = E/T + k_B \ln Z$. The sum of the lowest eigenvalue of all the vibrational modes defined the ZPE with anharmonic corrections.

4. Conclusions

After carefully analyzing the effect of the anharmonicity on the molecular vibrational model by explicitly calculating the DFT energies along all normal modes of a collection of Fe complexes, we can conclude the following. Firstly, the change in the ZPE upon the addition of the anharmonic effect was loosely related to the stiffness of the ligands coordinating the Fe ion. The HS-LS ZPE difference decreased most for the tridentate and bidentate ligands, whereas it increased slightly for the complex with the smallest monodentate ligand. Secondly, a tendency in the variation of the entropy was more difficult to reveal; both the ZPE and the spacing between the vibrational levels played a role in the final value of the entropy, and the effect was a subtle balance between these

two ingredients. Finally, we observed that the overall effect of the anharmonic correction was in general small enough to rely on the much simpler harmonic model, which gave direct estimates of the ZPE and ΔS without having to perform energy scans along the normal modes of the system under study. To proceed towards a computational strategy that is capable of reliably predicting transition temperatures for thermal spin crossover, it is more important to focus on a more sophisticated material model; environmental effects [64,65] and cooperativity [66,67] are expected to have a much larger influence than the anharmonic corrections.

References

1. Cambi, L.; Szego, L. The magnetic susceptibility of complex compounds. *Ber. Dtsch. Chem. Ges. B* **1931**, *64*, 2591–2598. [CrossRef]

2. Cambi, L.; Cagnasso, A. Iron dithiocarbamates and nitroso dithiocarbamates. *Atti. Accad. Naz. Lincei CI. Sci. Fis. Mat. Nut. Rend* **1931**, *13*, 809–813.

3. Hauser, A. Light-Induced spin-crossover and the high-spin → low-spin relaxation. In *Spin Crossover in Transition Metal Compounds II*; Gütlich, P., Goodwin, H.A., Eds.; Springer: Berlin/Heidelberg, Germany, 2004; Volume 234, pp. 155–198.

4. McGarvey, J.; Lawthers, I. Photochemically-induced perturbation of the 1A⇌5T equilibrium in FeII complexes by pulsed laser irradiation in the metal-to-ligand charge-transfer absorption band. *J. Chem. Soc. Chem. Commun.* **1982**, *16*, 906. [CrossRef]

5. Decurtins, S.; Gütlich, P.; Köhler, C.P.; Spiering, H.; Hauser, A. Light-Induced excited spin state trapping in a transition metal complex: The hexakis (1-propyltetrazole) iron(II) tetrafluoroborate spin-crossover system. *Chem. Phys. Lett.* **1984**, *105*, 1–4. [CrossRef]

6. Hauser, A. Intersystem crossing in the [Fe(ptz)$_6$](BF$_4$)$_2$ spin crossover system (ptz=1-propyltetrazole). *J. Chem. Phys.* **1991**, *94*, 2741–2748. [CrossRef]

7. Halcrow, M.A. The spin-states and spin-transitions of mononuclear iron(II) complexes of nitrogen-donor ligands. *Polyhedron* **2007**, *26*, 3523–3576. [CrossRef]

8. Dîrtu, M.M.; Rotaru, A.; Gillard, D.; Linares, J.; Codjovi, E.; Tinant, B.; Garcia, Y. Prediction of the Spin Transition Temperature in FeII One-Dimensional Coordination Polymers: An Anion Based Database. *Inorg. Chem.* **2009**, *48*, 7838–7852. [CrossRef] [PubMed]

9. Yamada, M.; Hagiwara, H.; Torigoe, H.; Matsumoto, N.; Kojima, M.; Dahan, F.; Tuchagues, J.P.; Re, N.; Iijima, S. A Variety of Spin-Crossover Behaviors Depending on the Counter Anion: Two-Dimensional Complexes Constructed by NH···Cl$^-$ Hydrogen Bonds, [Fe^{II}H$_3$L^{Me}]Cl·X (X = PF$_6$$^-$, AsF$_6$$^-$, SbF$_6$$^-$, CF$_3SO_3$$^-$; H$_3$L^{Me} = Tris[2-[(2- methylimidazol-4-yl)methylidene]aminoethyl]amine). *Chem. Eur. J.* **2006**, *12*, 4536–4549. [CrossRef] [PubMed]

10. Rodríguez-Velamazan, J.A.; Carbonera, C.; Castro, M.; Palacios, E.; Kitazawa, T.; Létard, J.F.; Burriel, R. Two-Step Thermal Spin Transition and LIESST Relaxation of the Polymeric Spin-Crossover Compounds Fe(X-py)$_2$[Ag(CN)$_2$]$_2$ (X=H, 3-methyl, 4-methyl, 3,4-dimethyl, 3-Cl). *Chem. Eur. J.* **2010**, *16*, 8785–8796. [CrossRef] [PubMed]

11. Bousseksou, A.; McGarvey, J.J.; Varret, F.; Real, J.A.; Tuchagues, J.P.; Dennis, A.C.; Boillot, M.L. Raman spectroscopy of the high- and low-spin states of the spin crossover complex Fe(phen)$_2$(NCS)$_2$: An initial approach to estimation of vibrational contributions to the associated entropy change. *Chem. Phys. Lett.* **2000**, *318*, 409–416. [CrossRef]

12. Wolny, J.A.; Paulsen, H.; Trautwein, A.X.; Schünemann, V. Density functional theory calculations and vibrational spectroscopy on iron spin-crossover compounds. *Coord. Chem. Rev.* **2009**, *253*, 2423–2431. [CrossRef]

13. Brehm, G.; Reiher, M.; Schneider, S. Estimation of the Vibrational Contribution to the Entropy Change Associated with the Low- to High-Spin Transition in Fe(phen)$_2$(NCS)$_2$ Complexes: Results Obtained by IR and Raman Spectroscopy and DFT Calculations. *J. Phys. Chem. A* **2002**, *106*, 12024–12034. [CrossRef]

14. Ronayne, K.L.; Paulsen, H.; Höfer, A.; Dennis, A.C.; Wolny, J.A.; Chumakov, A.I.; Schünemann, V.; Winkler, H.; Spiering, H.; Bousseksou, A.; et al. Vibrational spectrum of the spin crossover complex [Fe(phen)$_2$(NCS)$_2$] studied by IR and Raman spectroscopy, nuclear inelastic scattering and DFT calculations. *Phys. Chem. Chem. Phys.* **2006**, *8*, 4685–4693. [CrossRef] [PubMed]

15. Cirera, J.; Paesani, F. Theoretical Prediction of Spin-Crossover Temperatures in Ligand- Driven Light-Induced Spin Change Systems. *Inorg. Chem.* **2012**, *51*, 8194–8201. [CrossRef] [PubMed]

16. Rudavskyi, A.; Sousa, C.; de Graaf, C.; Havenith, R.W.A.; Broer, R. Computational approach to the study of thermal spin crossover phenomena. *J. Chem. Phys.* **2014**, *140*, 184318. [CrossRef] [PubMed]

17. Cirera, J.; Via-Nadal, M.; Ruiz, E. Benchmarking Density Functional Methods for Calculation of State Energies of First Row Spin-Crossover Molecules. *Inorg. Chem.* **2018**, *57*, 14097–14105. [CrossRef] [PubMed]

18. Siig, O.S.; Kepp, K.P. Iron(II) and Iron(III) Spin Crossover: Toward an Optimal Density Functional. *J. Phys. Chem. A* **2018**, *122*, 4208–4217. [CrossRef]

19. Kepp, K.P. Theoretical Study of Spin Crossover in 30 Iron Complexes. *Inorg. Chem.* **2016**, *55*, 2717–2727. [CrossRef]

20. Ye, S.; Neese, F. Accurate Modeling of Spin-State Energetics in Spin-Crossover Systems with Modern Density Functional Theory. *Inorg. Chem.* **2010**, *49*, 772–774. [CrossRef]

21. Swart, M. Spin States of (Bio)inorganic Systems: Successes and Pitfalls. *Int. J. Quantum Chem.* **2013**, *113*, 2–7. [CrossRef]

22. Swart, M. Accurate Spin-State Energies for Iron Complexes. *J. Chem. Theory Comput.* **2008**, *4*, 2057–2066. [CrossRef] [PubMed]

23. Jensen, K.P.; Cirera, J. Accurate Computed Enthalpies of Spin Crossover in Iron and Cobalt Complexes. *J. Phys. Chem. A* **2009**, *113*, 10033–10039. [CrossRef] [PubMed]

24. Kepp, K.P. Consistent descriptions of metal–ligand bonds and spin-crossover in inorganic chemistry. *Coord. Chem. Rev.* **2013**, *257*, 196–209. [CrossRef]

25. Staroverov, V.N.; Scuseria, G.E.; Tao, J.; Perdew, J.P. Comparative assessment of a new nonempirical density functional: Molecules and hydrogen-bonded complexes. *J. Chem. Phys.* **2003**, *119*, 12129–12137. [CrossRef]

26. Pierloot, K.; Vancoillie, S. Relative energy of the high-(^{5}T$_{2g}$) and low-(^{1}A$_{1g}$) spin states of [Fe(H$_2$O)$_6$]$^{2+}$, [Fe(NH$_3$)$_6$]$^{2+}$, and [Fe(bpy)$_3$]$^{2+}$: CASPT2 versus density functional theory. *J. Chem. Phys.* **2006**, *125*, 124303. [CrossRef] [PubMed]

27. Pierloot, K.; Vancoillie, S. Relative energy of the high-(^{5}T$_{2g}$) and low-(^{1}A$_{1g}$) spin states of the ferrous complexes [Fe(L)(NHS$_4$)]: CASPT2 versus density functional theory. *J. Chem. Phys.* **2008**, *128*, 034104. [CrossRef] [PubMed]

28. Vancoillie, S.; Zhao, H.; Radoń, M.; Pierloot, K. Performance of CASPT2 and DFT for Relative Spin-State Energetics of Heme Models Performance of CASPT2 and DFT for Relative Spin-State Energetics of Heme Models. *J. Chem. Theory Comput.* **2010**, *6*, 576–582. [CrossRef]

29. Ordejón, B.; de Graaf, C.; Sousa, C. Light-Induced Excited-State Spin trapping in Tetrazole-Based Spin Crossover Systems. *J. Am. Chem. Soc.* **2008**, *130*, 13961–13968. [CrossRef]

30. Lawson Daku, L.M.; Aquilante, F.; Robinson, T.W.; Hauser, A. Accurate Spin-State Energetics of Transition Metal Complexes. 1. CCSD(T), CASPT2, and DFT Study of [M(NCH)$_6$]$^{2+}$ (M = Fe, Co). *J. Chem. Theory Comput.* **2012**, *8*, 4216–4231. [CrossRef]

31. Barone, V.; Biczysko, M.; Bloino, J. Fully anharmonic IR and Raman spectra of medium-size molecular systems: accuracy and interpretation. *Phys. Chem. Chem. Phys.* **2014**, *16*, 1759–1787. [CrossRef]

32. Barone, V.; Biczysko, M.; Borkowska-Panek, M.; Bloino, J. A Multifrequency Virtual Spectrometer for Complex Bio-Organic Systems: Vibronic and Environmental Effects on the UV/Vis Spectrum of Chlorophyll a. *ChemPhysChem* **2014**, *15*, 3355–3364. [CrossRef] [PubMed]

33. Barone, V. Anharmonic vibrational properties by a fully automated second-order perturbative approach. *J. Chem. Phys.* **2005**, *122*, 014108. [CrossRef] [PubMed]

34. Escalera-Moreno, L.; Baldoví, J.J.; Gaita-Ariño, A.; Coronado, E. Spin states, vibrations and spin relaxation in molecular nanomagnets and spin qubits: A critical perspective. *Chem. Sci.* **2018**, *9*, 3265–3275. [CrossRef] [PubMed]

35. Liddle, S.T.; van Slageren, J. Improving f-element single molecule magnets. *Chem. Soc. Rev.* **2015**, *44*, 6655–6669. [CrossRef] [PubMed]

36. Escalera-Moreno, L.; Suaud, N.; Gaita-Ariño, A.; Coronado, E. Determining Key Local Vibrations in the Relaxation of Molecular Spin Qubits and Single-Molecule Magnets. *J. Phys. Chem. Lett.* **2017**, *8*, 1695–1700. [CrossRef] [PubMed]

37. Goodwin, C.A.P.; Ortu, F.; Reta, D.; Chilton, N.; Mills, D.P. Molecular magnetic hysteresis at 60 kelvin in dysprosocenium. *Nature* **2017**, *548*, 439–442. [CrossRef] [PubMed]

38. Ding, Y.S.; Yu, K.X.; Reta, D.; Ortu, F.; Winpenny, R.E.P.; Zheng, Y.Z.; Chilton, N. Field- and temperature-dependent quantum tunnelling of the magnetisation in a large barrier single-molecule magnet. *Nat. Commun.* **2018**, *9*, 3134. [CrossRef]

39. Lunghi, A.; Totti, F.; Sessoli, R.; Sanvito, S. The role of anharmonic phonons in under-barrier spin relaxation of single molecule magnets. *Nat. Commun.* **2017**, *8*, 14620. [CrossRef]

40. Yagi, K.; Hirao, K.; Taketsugu, T.; Schmidt, M.W.; Gordon, M.S. Ab initio vibrational state calculations with a quartic force field: Applications to H_2CO, C_2H_4, CH_3OH, CH_3CCH, and C_6H_6. *J. Chem. Phys.* **2004**, *121*, 1383–1389. [CrossRef]

41. Bloino, J.; Biczysko, M.; Barone, V. Anharmonic Effects on Vibrational Spectra Intensities: Infrared, Raman, Vibrational Circular Dichroism, and Raman Optical Activity. *J. Phys. Chem. A* **2015**, *119*, 11862–11874. [CrossRef]

42. Barnes, L.; Schindler, B.; Compagnon, I.; Allouche, A.R. Fast and accurate hybrid QM//MM approach for computing anharmonic corrections to vibrational frequencies. *J. Mol. Model.* **2016**, *22*, 285. [CrossRef] [PubMed]

43. Barnes, L.; Schindler, B.; Compagnon, I.; Allouche, A.R. iGVPT2: An interface to computational chemistry packages for anharmonic corrections to vibrational frequencies. *arXiv* **2017**, arXiv:1704.02144v1.

44. Domingo, A.; Carvajal, M.A.; de Graaf, C. Spin crossover in Fe(II) complexes: An ab initio study of ligand -donation. *Int. J. Quantum Chem.* **2010**, *110*, 331–337. [CrossRef]

45. Sorai, M. Calorimetric Investigations of Phase Transitions Occurring in Molecule-Based Materials in Which Electrons Are Directly Involved. *Bull. Chem. Soc. Jpn.* **2001**, *74*, 2223–2253. [CrossRef]

46. Gallois, B.; Real, J.A.; Hauw, C.; Zarembowitch, J. Structural Changes Associated with the Spin Transition in Fe(phen)$_2$(NCS)$_2$:A Single-Crystal X-ray Investigation. *Inorg. Chem.* **1990**, *29*, 1152–1158. [CrossRef]

47. Reiher, M.; Salomon, O.; Hess, A. Reparameterization of hybrid functionals based on energy differences of states of different multiplicity. *Theor. Chem. Acc.* **2001**, *107*, 48–55. [CrossRef]

48. Reiher, M. Theoretical Study of the Fe(phen)$_2$(NCS)$_2$ spin-crossover coplex with reparametrized Density functionals. *Inorg. Chem.* **2002**, *41*, 6928–6935. [CrossRef]

49. Sellmann, D.; Soglowek, W.; Knoch, F.; Ritter, G.; Dengler, J. Transition-Metal Complexes with Sulfur Ligands. 88.* 1 Dependence of Spin State, Structure, and Reactivity of [Fe^{II}(L)('NHS$_4$')] Complexes on the Coligand L (L = CO, N_2H_2, N_2H_4, NH_3, Pyridine, NHCH$_3$NH$_2$, CH_3OH, THF, P(OCH$_2$)$_3$, P(OPh)$_3$): Model Complexes for Iron Nitrogenases ('NHS$_4$'$^{2-}$ = Dianion of 2,2'-Bis[(2-mercaptophenyl)thio]diethylamine). *Inorg. Chem.* **1992**, *31*, 3711–3717.

50. Gruden, M.; Stepanović, S.; Swart, M. Spin state relaxation of iron complexes: The case for OPBE and S12g. *J. Serb. Chem. Soc.* **2015**, *80*, 1399–1410. [CrossRef]

51. Guionneau, P.; Le Gac, F.; Kaiba, A.; Sánchez Costa, J.; Chasseau, D.; Létard, J.F. A reversible metal–ligand bond break associated to a spin-crossover. *Chem. Commun.* **2007**, 3723–3725. [CrossRef]

52. Dose, E.V.; Murphy, K.M.M.; Wilson, L.J. Synthesis and Spin-State Studies in Solution of 7-Substituted Tris(l8-diketonato)iron(III) Complexes and Their Spin-Equilibrium /3-Ketoimine Analogues Derived from Triethy lenetetramine. *Inorg. Chem.* **1976**, *15*, 2622–2630. [CrossRef]

53. Hinek, R.; Gütlich, P.; Hauser, A. Cooperative effects in the [Fe(mtz)$_6$](BF$_4$)$_2$ Spin-Crossover system: Fine tuning the energy gap. *Inorg. Chem.* **1994**, *33*, 567–572. [CrossRef]

54. Kusz, J.; Spiering, H.; Gütlich, P. X-ray structure study of the light-induced metastable states of the spin-crossover compound [Fe(mtz)$_6$](BF$_4$)$_2$. *J. Appl. Crystallogr.* **2001**, *34*, 229–238. [CrossRef]

55. Hibbs, W.; van Koningsbruggen, P.J.; Arif, A.M.; Shum, W.W.; Miller, J.S. One- and Two-Step Spin-Crossover Behavior of $[Fe^{II}(isoxazole)_6]^{2+}$ and the Structure and Magnetic Properties of Triangular $[Fe^{III}_3O(OAc)_6(isoxazole)_3][ClO_4]$. *Inorg. Chem.* **2003**, *42*, 5645. [CrossRef] [PubMed]

56. Nakamoto, T.; Tan, Z.C.; Sorai, M. Heat Capacity of the Spin Crossover Complex $[Fe(2\text{-}pic)_3]Cl_2 \cdot MeOH$: A Spin Crossover Phenomenon with Weak Cooperativity in the Solid State. *Inorg. Chem.* **2001**, *40*, 3805–3809. [CrossRef]

57. Köppen, H.; Müller, E.W.; Köhler, C.P.; Spiering, H.; Meissner, E.; Gütlich, P. Unusual spin-transition anomaly in the spin crossover system $[Fe(2\text{-}pic)_3]Cl_2 \cdot EtOH$. *Chem. Phys. Lett.* **1982**, *91*, 348–352. [CrossRef]

58. Neese, F. Software update: The ORCA program system, version 4.0. *WIREs Comput. Mol. Sci.* **2018**, *8*. [CrossRef]

59. Weigend, F.; Ahlrichs, R. Balanced basis sets of split valence, triple zeta valence and quadruple zeta valence quality for H to Rn: Design and assessment of accuracy. *Phys. Chem. Chem. Phys.* **2005**, *7*, 3297–3305. [CrossRef]

60. Neese, F.; Wennmohs, F.; Hansen, A.; Becker, U. Efficient, approximate and parallel Hartree–Fock and hybrid DFT calculations. A 'chain-of-spheres' algorithm for the Hartree–Fock exchange. *Chem. Phys.* **2009**, *356*, 98–109. [CrossRef]

61. Petrenko, T.; Kossmann, S.; Neese, F. Efficient time-dependent density functional theory approximations for hybrid density functionals: Analytical gradients and parallelization. *J. Chem. Phys.* **2011**, *134*, 054116. [CrossRef]

62. Latouche, C.; Palazzetti, F.; Skouteris, D.; Barone, V. High-Accuracy Vibrational Computations for Transition-Metal Complexes Including Anharmonic Corrections: Ferrocene, Ruthenocene, and Osmocene as Test Cases. *J. Chem. Theory Comput.* **2014**, *10*, 4565–4573. [CrossRef] [PubMed]

63. Aquilante, F.; Autschbach, J.; Carlson, R.K.; Chibotaru, L.; Delcey, M.G.; De Vico, L.; Fernández-Galván, I.; Ferré, N.; Frutos, L.M.; Gagliardi, L.; et al. MOLCAS 8: New Capabilities for Multiconfigurational Quantum Chemical Calculations across the Periodic Table. *J. Comput. Chem.* **2016**, *37*, 506–541. [CrossRef] [PubMed]

64. Vela, S.; Fumanal, M.; Ribas-Ariño, J.; Robert, V. Towards an accurate and computationally-efficient modelling of Fe(II)-based spin crossover materials. *Phys. Chem. Chem. Phys.* **2015**, *17*, 16306–16314. [CrossRef] [PubMed]

65. Fumanal, M.; Jiménez-Grávalos, F.; Ribas-Ariño, J.; Vela, S. Lattice-Solvent Effects in the Spin-Crossover of an Fe(II)-Based Material. The Key Role of Intermolecular Interactions between Solvent Molecules. *Inorg. Chem.* **2017**, *56*, 4474–4483. [CrossRef] [PubMed]

66. Kreutzberg, L.; Hübner, C.G.; Paulsen, H. Cooperativity of Spin Crossover Complexes: Combining Periodic Density Functional Calculations and Monte Carlo Simulations. *Materials* **2017**, *10*, 172. [CrossRef] [PubMed]

67. Bertoni, R.; Collet, E.; Cailleau, H.; Boillot, M.L.; Tissot, A.; Laisney, J.; Enachescu, C.; Lorenc, M. Temperature dependence of the cooperative out-of-equilibrium elastic switching in a spin-crossover material. *Phys. Chem. Chem. Phys.* **2019**, *21*, 6606–6612. [CrossRef] [PubMed]